 doi:10.20944/preprints202110.0374.v1

High Level Oxygen Reduction Catalysts Derived from the Compounds of Large Specific Surface Area Pine Peel Activated Carbon and Phthalocyanine Cobalt

Lei Zhao[1+*], Ziwei Lan[1+], Junyu Su[1], Huazhu Liang[1], Jiayu Yao[1], Wenhao Mo[1], Wenhu Yang[2*]

[+]*equal contribution in this paper.*

**Corresponding authors.*

[1]*Department of physical science and technology, Lingnan Normal University, Zhanjiang 524048, PR China, E-mail: leizhaolingnan@163.com (L. Zhao)*

[2]*School of Electronics and Information Engineering, Guangdong Ocean University, Zhanjiang 524088, PR China, E-mail: yangwenhu@stu.gdou.edu.cn (W. Yang).*

Preprints (www.preprints.org) | NOT PEER-REVIEWED | Posted: 26 October 2021 doi:10.20944/preprints202110.0374.v1

Abstract

Compared with precious metal catalysts, non-platinum catalysts have the advantages of low cost and high performance. Among them, the activated carbon (AC) with a large specific surface area (SSA) can be used as a carrier or as a carbon source of nonprecious metal/carbon system catalyst at the same time. Therefore, this paper uses cheap pine peel bio-based materials to prepare large surface area activated carbon and then compound with cobalt phthalocyanine (CoPc) to obtain a high-performance cobalt/nitrogen/carbon catalyst. The merits include AC@CoPc composite catalysts are prepared by precisely controlling the composite proportion of AC and CoPc, the atomically dispersed Co nanoparticles form and synergistically with N promote the exposure of CoN_x active sites, and the E_{onset} of the catalyst treated with a composite proportion of AC and CoPc of 1 to 2 at 800 °C (AC@CoPc-800-1-2) is 1.01 V, which is higher than Pt/C (20 wt%) catalyst. Apart from this, the stability is 87.8% in 0.1 M KOH after 20000 s testing in compared with other AC@CoPc series catalysts and Pt/C (20 wt%) catalyst. Considering from the performance and price of the catalyst in practical application, these composite catalysts combine biomass carbon materials with phthalocyanine series, which will be widely used in the area of nonprecious metal catalysts.

Keywords: Oxygen reduction reaction; Nanoporous activated carbon; Cobalt-nitrogen-doped carbon; Nonprecious metal catalyst

1. Introduction

Environmental pollution and foreseeable energy shortages have become a tricky problem, so pollution-free and renewable energy technology is of paramount importance to mankind today[1-3]. The oxygen reduction reaction (ORR) is a critical central reaction in fuel cells and metal-air batteries, but fuel cells are always limited for the sluggish of ORR at cathode[4-6]. Nowadays, the predominant commercial ORR catalysts are still Pt and its alloys because of their high properties. However, Pt and its alloys, which is expensive and scarce in resources, greatly limits their practical applications[7-9].

 doi:10.20944/preprints202110.0374.v1

In recent years, in order to overcome the shortcomings of Pt-based catalysts, many nonprecious metal ORR catalysts with high electrocatalytic activity have been explored, including metal hydroxides[10], oxides[11], sulfides[12], phosphides[13], nitrides[14], selenides[15], and heteroatoms doped carbon materials[16-18]. Among them, heteroatoms doped carbon materials are very effective in improving the catalytic activity of ORR for the large SSA and lots of catalytic sites[19]. Doping carbon with heteroatoms (especially N) can improve the charge distribution of adjacent C atoms to provide high catalytic activity and high stability[20]. Because of the existence of pyridine and pyrrole-like N species, N-doped carbon materials exhibit excellent catalytic activity, and the higher the content of pyridine dinitrogen and pyrrole nitrogen, the more beneficial the improvement of ORR catalytic activity[21,22]. Besides, transition metals (for example, Co, Fe, and Ni) also have a pivotal role in ORR, but the scarcity of active sites and low electron transfer efficiency restrict their catalytic activity. And the M-N-C composite catalyst composed of N-doped carbon materials and transition metal has been widely studied for its ability to enrich abundant active sites and improve the conductivity and the strong synergy between the composition[23-25]. Recently, a predominant direction in the series of M-N-C is phthalocyanines metal catalyst, especially CoPc, which have shown prominent catalytic effect for reducing molecular oxygen and four-electron pathway[26]. However, in order to solve the problem of low conductivity of CoPc, various carbon materials have been compounded with CoPc to enhance the overall electrochemical performance of composite materials including carbon nanotubes[27] and graphene[28]. Compared with many carbon materials, biomass-derived carbon materials have been developed as a low-cost nonprecious metal catalyst thanks to their high availability, accessibility and recyclability. Biomass pine peels are widely distributed throughout China and are freely available, which will provide a good foundation for the development and application of nonprecious metal N-doped carbon catalysts. Simultaneously, to promote the formation of catalytic sites to enhance catalytic performance, the most critical step is to design a catalyst with a large SSA and abundant nanopores to promote high mass transfer flux and high catalytic activity[29],

Preprints (www.preprints.org) | NOT PEER-REVIEWED | Posted: 26 October 2021 doi:10.20944/preprints202110.0374.v1

which can be done by adjusting the concentration of the activator and the activation temperature[30]. Therefore, it is desirable to design and prepare Co-N-C catalysts with high electrocatalytic activity by converting N-doped pine peel into nanocarbon through pre-activation and heat treatment to regulate the chemical structure and morphology of carbon, and then conduct pyrolysis with an appropriate proportion of CoPc at high temperature. Compared with other precursors containing nitrogen and cobalt (such as aniline[31], melamine[32], pyrrole[33] and metal organic frameworks[34]), this method is simpler, more effective, lower cost, and more promising to prepare Co-N-C catalysts with synergistic effect and significantly enhanced ORR catalytic activity.

Herein, we synthesized a series of AC@CoPc composite catalysts through pre-activation treatment, high-temperature carbonization methods and precise control the composite proportion of AC derived from biomass pine peel and CoPc. And the characterization analysis and electrochemical study of AC@CoPc series composite catalysts under different composite proportions and temperature conditions were also carried out. Compared with other AC@CoPc series catalysts and Pt/C (20 wt%) catalysts, AC@CoPc-800-1-2 had excellent catalytic ability for ORR, which benefited from AC derived from biomass pine peel with a large SSA and many nanopores provided abundant particle attachment sites, N-doped activated carbon improved the charge distribution of adjacent C atoms and generated more charge sites as well as the formation of an enormous number of atomically dispersed Co nanoparticles encapsulated by graphitic carbon and synergistically with N promote the exposure of CoN_x active sites.

2. Experimental

All reagents are analytically pure and can be used without further purification.

2.1. Preparation of AC@CoPc series composite catalysts

2.1.1 Preparation of AC

The pine peel was obtained locally in Harbin, China, washed by distilled water and crushed. First, the pine peel was mixed with KOH at a mass ratio of 1:4 and then heated at 900 ℃ for 1 h in tubular furnace with the heating rate of 5 ℃

Preprints (www.preprints.org) | NOT PEER-REVIEWED | Posted: 26 October 2021 doi:10.20944/preprints202110.0374.v1

min^{-1} under N_2 atmosphere with the flowing rate of 100 ml min^{-1}. After activated, the above samples were washed with 1 M HCl and distilled water several times and dried for 12 h at 60 °C. Finally, the obtained samples were denominated as AC.

2.1.2 Preparation of AC@CoPc

The cobalt phthalocyanine compound was purchased from Shanghai, China. To obtain AC@CoPc series composite catalysts, AC and CoPc were mixed with the mass ratio of 2:1, 1:1, and 1:2 by carbonizing at 700, 800, and 900 °C for 1 h in a N_2 atmosphere, respectively. Then the obtained samples were grinded for 1 h with ethanol solution in the glass dish, and dried for 12 h at 60 °C. Scheme 1 is a schematic illustration of AC@CoPc series composite catalysts. The AC@CoPc series composite catalysts were named as self-defined pattern, such as the composed materials of AC and CoPc mixed with the mass ratio of 2:1 was dominated as AC@CoPc-700-2-1.

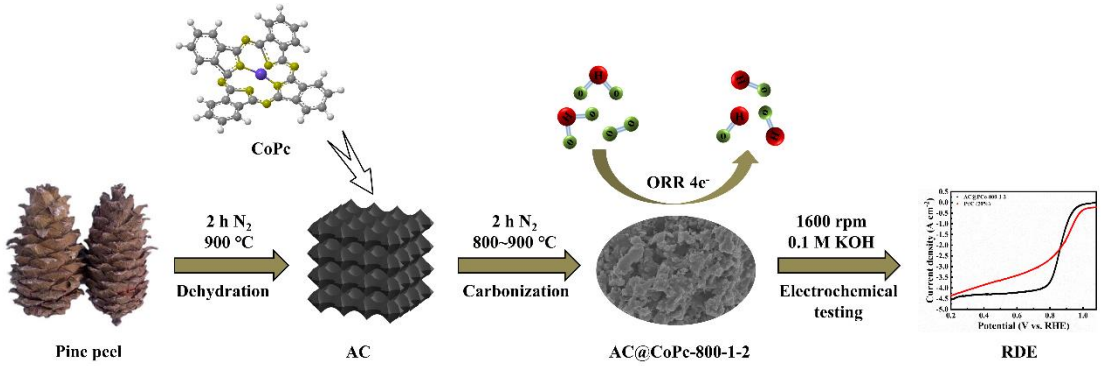

Scheme 1 The schematic illustration of the synthesis of AC@CoPc series catalysts.

2.2 Structure characterizations

Scanning electron microscopy (SEM, Hitachi S-4800) was used to investigate the surface morphology and structure of the catalyst samples. X-ray diffraction (XRD) patterns of the samples were obtained on a Shimadzu XRD-6000 X-ray diffractometer using Cu K_a radiation with 4°min^{-1}. Transmission electron microscopy (TEM) and selected area mapping were collected were operated on a JEM-2100F instrument with acceleration voltage of 100 kV. X-ray photoelectron spectroscopy (XPS) analysis was investigated using a VG Scientific ESCALAB 250 iXL spectrometer with an Al K_a X-ray source.

Preprints (www.preprints.org) | NOT PEER-REVIEWED | Posted: 26 October 2021 doi:10.20944/preprints202110.0374.v1

2.3 Electrochemical characterizations

Electrochemical experiments were conducted at room temperature on an electrochemical workstation (RST5200F, Zhengzhou shiruisi Instrument Co., Ltd. China). Linear sweep voltammetry (LSV) and rotating-disk electrode (RDE) polarization curves were measured in a conventional three-electrode electrochemical system. And, platinum wire (CHI115) electrode and Ag/AgCl (sat.) (CHI111) electrode were used as counter electrode and reference electrode, respectively. A glassy carbon (GC) electrode (5 mm in diameter, 0.196 cm^2) was used for the working electrode to test the LSV and RDE curves, respectively. Before measurements, the GC electrodes were carefully polished with gamma alumina powders (0.05 mm) until a mirror-like surface was obtained, and then washed with distilled water twice and dried in vacuum. Subsequently, the AC@CoPc series composite catalysts (400 μg cm^{-2}) were put onto the GC electrode followed by dripping a drop of Nafion solution (5 wt. %, Dupont), improving the adhesion of active materials and the GC electrode surface. All electrode potentials in this work were quoted versus a reversible hydrogen electrode (vs. RHE), and a potential of 0.989 V was added to the conversion with RHE. RDE experiments for ORR were performed over the potential range of 0.2~1.1 V in O_2-saturated 0.1 M KOH solution at the scan rate of 10 mV s^{-1}. The RDE polarization curves were measured by the reference electrode of Ag/AgCl (sat.) in 0.1 M KOH solution at the scan rate of 10 mV s^{-1} and rotation rates from 400 to 1600 rpm. The measurement of the current-time (i-t) curves were used to evaluate the stability of the catalyst at a constant potential of 0.6 V (vs. RHE) for 20000s, in which O_2 was bubbled at a continuous flow rate of 20 mL min^{-1} at the rotation rate of 1600 rpm. Under the same experimental conditions, Pt/C (20 wt%) purchased from Shanghai He Sen Electric Co., Ltd. was used for the above experimental comparison.

2.4 Calculation of electron transfer number (n)

The electron transfer number (n) is determined by the Koutecky-Levich equation at a series of potentials:

$$\frac{1}{J} = \frac{1}{J_L} + \frac{1}{J_K} = \frac{1}{B\omega^{1/2}} + \frac{1}{J_K}$$

Preprints (www.preprints.org) | NOT PEER-REVIEWED | Posted: 26 October 2021 doi:10.20944/preprints202110.0374.v1

$$B = 0.62\, n\, F\, C_0\, (D_0)^{2/3}\, v^{-1/6}$$

$$J_K = n\, FkC_0$$

Where J is the measured current density (mA cm^{-2}), J_L and J_K are the diffusion-limiting and kinetic current densities (mA cm^{-2}), ω is the angular velocity of the disk ($\omega = 2\pi N$, N is the linear rotation speed), n is the overall number of electrons transferred per oxygen molecule during ORR, D_0 is the diffusion coefficient (cm s^{-1}), F is the Faraday constant (F = 96486.4 C mol^{-1}), C_0 is the bulk concentration of O_2 (mol L^{-1}), v is the kinematic viscosity of the electrolyte, k is the electron transfer rate constant, and the values of C_0, D_0 and v for O_2-saturated 0.1 M KOH solution are 1.20×10^{-6} mol cm^{-3}, 1.90×10^{-5} cm^2 s^{-1}, and 0.01 cm^2 s^{-1}, respectively.

3. Results and discussion

The SEM images of AC and different proportion AC@CoPc series composite catalysts are shown in Figure 1 and Figure 2. In Figure 1b and 1e, it can be observed that the surface is covered with many nanopores, showing a feature of few particles and more nanopores. This should be due to the low proportion of composite CoPc, which generally shows a basic nanoporous structure, such as AC (Figure 1a). As the temperature and the proportion of composite CoPc increase, the surface nanoporous structure gradually decreases, and the particles attached to the surface gradually increase (Figure 1b-h), where AC@CoPc-800-2-1 (Figure 1g) shows a uniform distribution. As can be seen from Figure 2, with the increase of temperature, CoPc compound can prevent the formation of nanoporous structure, and the SSA will also change during the heating process of 700~900 ℃ (Figure 2a-h). Compared with AC@CoPc-900-1-2 (Figure 2h), AC@CoPc-800-1-2 (Figure 2e) has a better composite degree of AC and CoPc, with more uniform distribution and larger SSA. These results suggest that the rich distribution and size of nanopores can be regulated and controlled by pyrolysis temperature and activation, thereby forming more nanopores to expose more active areas and promote the ability of electron transfer[35,36], but the appropriate temperature and proportion are more conducive to the recombination of AC and CoPc as well as can provide more adhesion sites for CoPc.

Preprints (www.preprints.org) | NOT PEER-REVIEWED | Posted: 26 October 2021 doi:10.20944/preprints202110.0374.v1

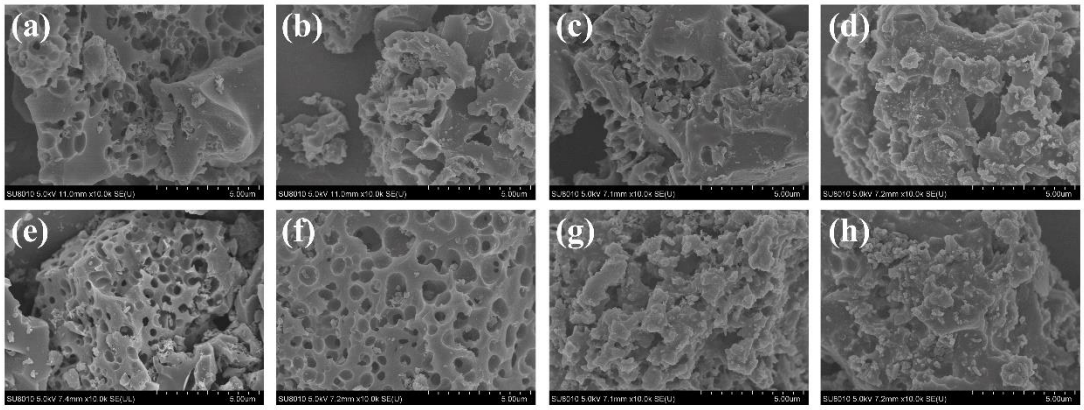

Figure 1 SEM images with low magnification: (a) AC, (b) AC@CoPc-700-2-1, (c) AC@CoPc-700-1-1, (d) AC@CoPc-700-1-2, (e) AC@CoPc-800-2-1, (f) AC@CoPc-800-1-1, (g) AC@CoPc-800-1-2 and (h) AC@CoPc-900-1-2.

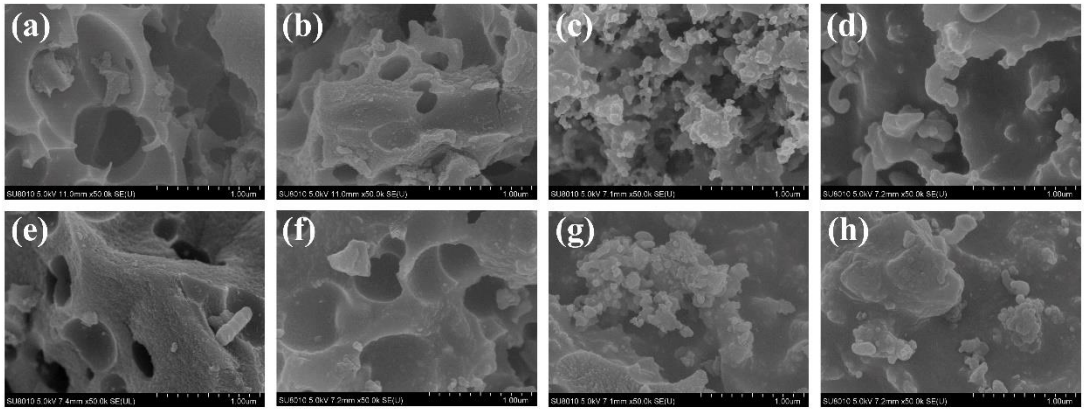

Figure 2 SEM images with high magnification: (a) AC, (b) AC@CoPc-700-2-1, (c) AC@CoPc-700-1-1, (d) AC@CoPc-700-1-2, (e) AC@CoPc-800-2-1, (f) AC@CoPc-800-1-1, (g) AC@CoPc-800-1-2 and (h) AC@CoPc-900-1-2.

The XRD patterns of AC@CoPc series composite catalysts (Figure 3a) all correspond to Co (JCPDS 15-0806)[37] and graphite (JCPDS 01-0646)[38]. AC@CoPc-800-1-2 and AC@CoPc-900-1-2 exhibit that the broaden peak at 25.7° is ascribed to the (002) plane of graphite (JCPDS 01-0646), but AC@CoPc-800-1-2 has a larger broad peak at 25.7°, which manifests that the carbonization temperature of 800 ℃ is more conducive to the formation of carbon with small graphite domains[39]. Moreover, the peaks of AC@CoPc series composite catalysts at 44.2° and 51.5° can be indexed to the (111) and (200) plane of Co (JCPDS 15-0806), indicating that CoPc has been transformed into metallic cubic-phase Co nanoparticles under high temperature pyrolysis, which can be reflected from the following XPS analysis.

Preprints (www.preprints.org) | NOT PEER-REVIEWED | Posted: 26 October 2021 doi:10.20944/preprints202110.0374.v1

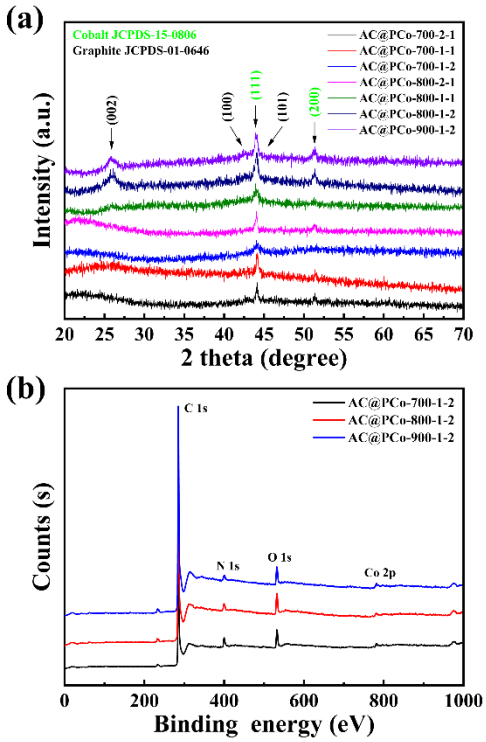

Figure 3 (a) The XRD patterns of AC@CoPc series catalysts, (b) the XPS survey spectra of AC@CoPc-700-1-2, AC@CoPc-800-1-2 and AC@CoPc-900-1-2.

TEM was used to further characterize the structural details of AC@CoPc-800-1-2. In Figure 4a, many vague small black spots are exposed as active sites on the carbon skeleton, and they are uniformly distributed. HRTEM images of Figure 4c confirmed that these active sites (circled in yellow circles in Figure 4b) are Co nanoparticles active sites with a lattice spacing of 0.20 nm corresponding to (111) crystal plane of Co, which have been embedded into the carbon skeleton, while 0.33 nm corresponds to the (002) crystal plane of graphite[40]. This value is larger than the spacing of (002) in graphite, showing a disordered effect in the catalyst, and the graphite carbon tightly wraps the active sites of Co nanoparticles in the carbon skeleton, which also enhances the mechanical stability of nanostructured composites[41,42]. The element mappings (Figure 4d) display the good dispersion of C, O, N and Co, which is the result of the N-doped carbon with interspersed Co.

Preprints (www.preprints.org) | NOT PEER-REVIEWED | Posted: 26 October 2021 doi:10.20944/preprints202110.0374.v1

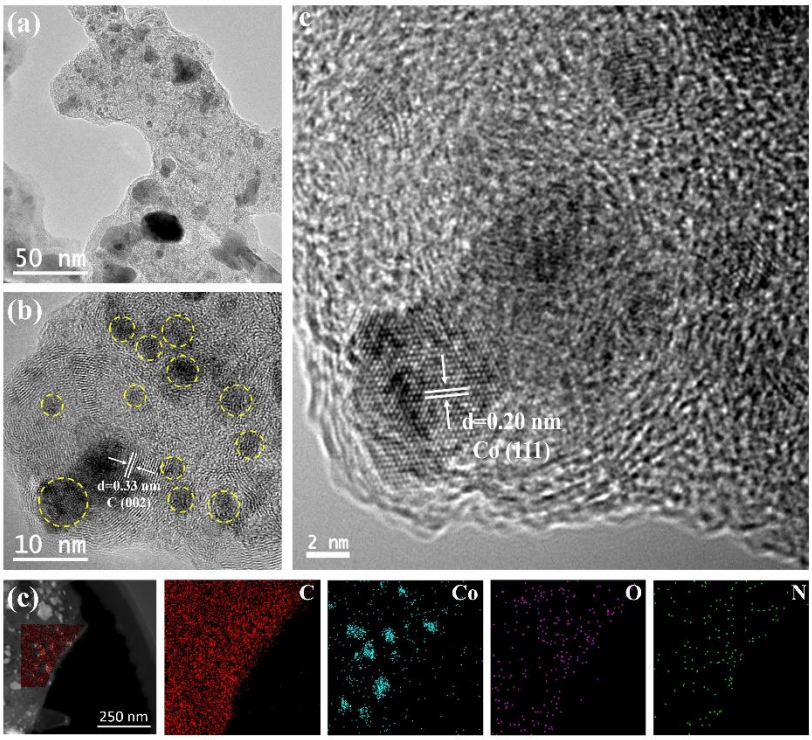

Figure 4 (a, b) The TEM and (c) HRTEM images of AC@CoPc-800-1-2 and (d) the corresponding elemental mapping analysis of AC@CoPc-800-1-2.

The XPS spectra of AC@CoPc-700-1-2, AC@CoPc-800-1-2 and AC@CoPc-900-1-2 are given in Figure 3b, including four elements C, O, N and Co. The major part of N moieties in AC@CoPc-700-1-2 (Figure 5a) is 54.87% but two peaks at 399.7 eV (N2, CoN_x) and 400.9 eV (N3, pyrrolic-N) are relatively lower in compared with AC@CoPc-800-1-2 (Figure 5c). And other two peaks at 401.3 eV and reported in the literature from 397 to 399.5 eV are assigned to graphitic-N (N4) and pyridinic-N (N1)[43]. While the major part of nitrogen moieties in AC@CoPc-800-1-2 exhibits the higher contribution of pyridine-N and a high amount of Co and N association in the CoN_x structure. Except the two catalysts mentioned above, AC@CoPc-900-1-2 shows lower CoN_x and pyrrolic-N content in Table 1. Therefore, we have reason to infer that pyridine-N sites and CoN_x have a substantial role in ORR. For Co 2p, the XPS spectra of these three composite catalysts (Figure 5b) show that three main peaks at 780.3 eV, 781.8 eV, and around 783 eV are assigned to Co, Co_xO_y or CoC_xN_y, and CoN_x respectively[44-46]. The cobalt content percentages of these three composite catalysts are 0.77%, 0.52%, and 0.51%, respectively. As the temperature increased, the cobalt content gradually decreased, while the nitrogen content is 6.63%, 3.35% and 2.91%, also showing a downward trend (Figure 5d). This

Preprints (www.preprints.org) | NOT PEER-REVIEWED | Posted: 26 October 2021 doi:10.20944/preprints202110.0374.v1

indicates that high temperature (800 °C) can increase the reaction rate between Co and N, but too high temperature (900 °C) will cause a large loss of N. And compared with AC@CoPc-700-1-2 and AC@CoPc-900-1-2, cobalt content in AC@CoPc-800-1-2 shows higher CoN_x content and the result is consistent with the analysis of N2 moiety.

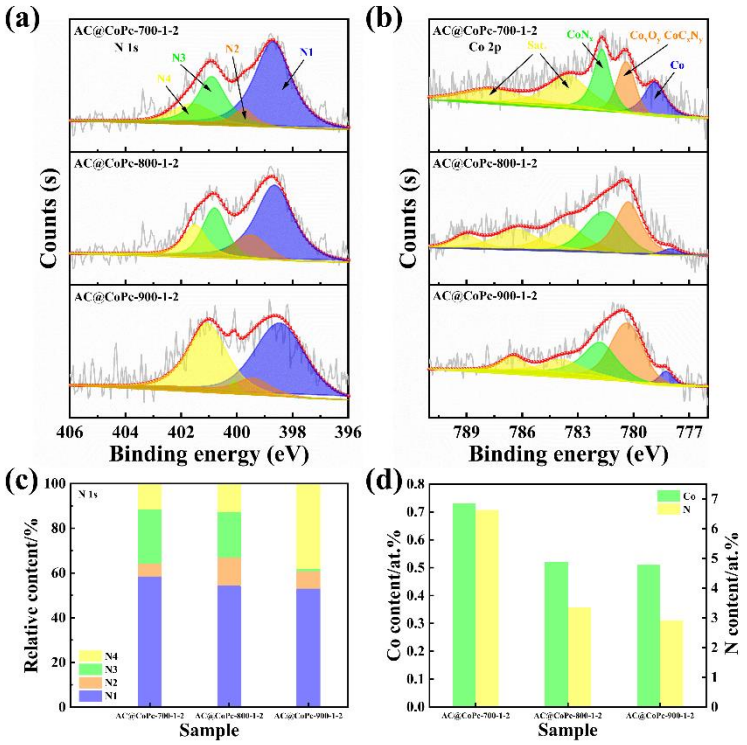

Figure 5 The XPS spectra of (a) N 1s, (b) Co 2p, (c) the relative contents of different N species obtained from fitting of XPS spectra of N 1s and (d) surface content of N and Co obtained from XPS survey spectra for AC@CoPc-700-1-2, AC@CoPc-800-1-2 and AC@CoPc-900-1-2.

Table 1 Ration analysis of the peaks in XPS spectra in AC@CoPc series catalysts.

	Element contents (at%)							
Catalysts	**C**	**O**	**Co**	**N total**	**N1**	**N2**	**N3**	**N4**
AC@CoPc-700-1-2	85.19	7.45	0.73	6.63	58.47	5.64	24.31	11.58
AC@CoPc-800-1-2	90.04	6.09	0.52	3.35	54.29	12.61	20.33	12.76
AC@CoPc-900-1-2	92.02	4.56	0.51	2.91	53.04	7.79	1.07	38.10

In order to identify the properties of catalysts in Figure 6a, Table 2 contrasted the parameters of AC@CoPc-800-1-2 (the best ORR catalyst in AC@CoPc series composite catalysts) and Pt/C (20 wt%) catalyst. The difference between the ORR activities of AC@CoPc series composite catalysts was compared, including E_{onset}, $E_{1/2}$ as well as the current density of 0.95, 0.90, 0.85 and 0.80 V. As shown in Figure 6a,

Preprints (www.preprints.org) | NOT PEER-REVIEWED | Posted: 26 October 2021 doi:10.20944/preprints202110.0374.v1

the E_{onset} of AC@CoPc-800-1-2 is 1.01 V, which is higher than Pt/C (20 wt%) catalyst with the onset potential of 0.989V. These results demonstrate that except for the limited current density (Figure 6b), the AC@CoPc series composite catalysts show better catalyst effects than Pt/C (20 wt%) catalysts. The LSV curves at different rotating speeds are tested to further evaluate ORR performance of AC@CoPc-800-1-2 (Figure 6c), and the corresponding K-L plots are given in Figure 6d. The K-L plots show the good linearity and parallelism, indicating that the ORR process of the AC@CoPc-800-1-2 follows first-order kinetics in the selected potential range from 0.50 to 0.70 V (vs. RHE). The electron transfer numbers (n) transferred during ORR and the kinetic limited current density (J_k) can be calculated from the following K-L equation[47,48]. Transfer electron numbers (n) of AC@CoPc-800-1-2 from 0.50 to 0.70 V in Figure 7d are all around four electrons, showing high four-electron pathway. The stable testing results of AC@CoPc-800-1-2 and commercial Pt/C (20 wt%) catalyst was evaluated by i-t curve at a constant potential of 0.6 V (vs. RHE) with a disk rotating rate of 1600 rpm (Figure 6e). After 20000 s testing, the stability of AC@CoPc-800-1-2 is 87.8%, which is much higher than commercial Pt/C (20 wt%) catalyst with only 82.1% stability. Furthermore, the E_{onset} (vs. RHE) and $E_{1/2}$ (vs. RHE) of AC@CoPc-800-1-2 are comparable to that of various Co-N-C catalysts in 0.1 M KOH (Figure 6f), as listed in Table 3.

Preprints (www.preprints.org) | NOT PEER-REVIEWED | Posted: 26 October 2021 doi:10.20944/preprints202110.0374.v1

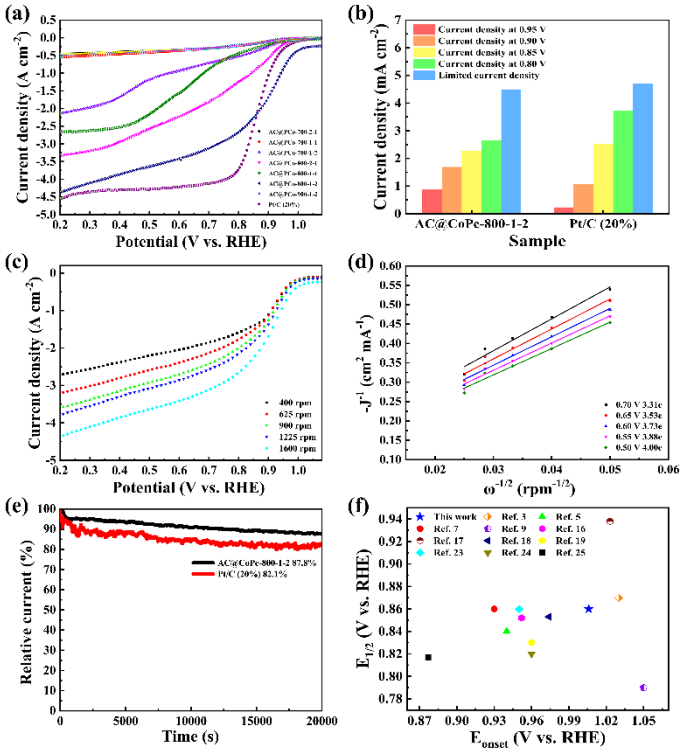

Figure 6 (a) RDE curves of AC@CoPc series catalysts and Pt/C (20 wt%) catalyst at the rotation speed of 1600 rpm with the scan rate of 5 mV s^{-1} in O_2 saturated 0.1 M KOH, (b) the Current density at 0.80~0.95 V (vs. RHE) and limited current densities at 0.30 V (vs. RHE) of AC@CoPc-800-1-2 and Pt/C (20 wt%) catalyst, (c) LSV curves of AC@CoPc-800-1-2 at different rotation speeds from 400 rpm to 1600 rpm with the scan rate of 5 mV s^{-1} in O_2 saturated 0.1 M KOH, (d) the corresponding K-L plots ($-J^{-1}$ vs. $\omega^{-1/2}$) at different potential in O_2 saturated 0.1 M KOH, (e) stable testing results of AC@CoPc-800-2-1 and Pt/C (20 wt%) catalyst at 0.60 V (vs. RHE) and (f) the comparison of the onset potential (V vs. RHE) and half-wave potential (V vs. RHE) in 0.1 M KOH of AC@CoPc-800-1-2 with other recent three years reported Co-N-C catalysts.

Table 2 Comparison of ORR parameters between AC@CoPc-800-1-2 and Pt/C (20 wt%) catalyst.

Catalyst	E_{onset} (V vs RHE)	$E_{1/2}$ (V vs RHE)	Current density at 0.95V (mA cm^{-2})	Current density at 0.90V (mA cm^{-2})	Current density at 0.85V (mA cm^{-2})	Current density at 0.80V (mA cm^{-2})	Limited current density (mA cm^{-2})
AC@CoPc-800-1-2	1.006	0.860	0.869	1.688	2.264	2.658	4.50
Pt/C (20%)	0.989	0.858	0.2322	1.060	2.524	3.722	4.70

Preprints (www.preprints.org) | NOT PEER-REVIEWED | Posted: 26 October 2021 doi:10.20944/preprints202110.0374.v1

Table 3 Comparison of the content and source of N and Co and ORR catalytic activity of Co-N-C catalysts with values from the literature of the recent three years.

Catalysts	The content and source of Co and N (at.%)	E_{onset} (V vs. RHE)	$E_{1/2}$ (V vs. RHE)	Limited current density (mA cm^{-2})	Average transferred electron number (n)	Durability	Ref.
AC@CoPc-800-1-2	**0.52, 3.35 CoPc pine peel**	**1.006**	**0.860**	**4.50**	**3.69**	**20000s/87.8%**	**This work**
Co-N-C-800	0.83, 2.94 $Co(NO_3)_2·6H_2O$ 2-methylimidazole	1.030	0.870	5.52	3.97	72000s/92%	[3]
Co-NC-700	1.07, 4.46 $Co(Ac)_2·4H_2O$ 1,10-phenanthroline	0.940	0.840	6.30	3.89	$\Delta E_{1/2}$= −5 mV (10000 cycles)	[5]
ZIF/ppy-pani-750	1.23, 11.21 $Co(NO_3)_2·6H_2O$ ppy-pani	0.930	0.860	4.99	3.82	64800 s/88.73%	[7]
ECo@D	0.041, 5.23 EDTA-Co DA	1.050	0.790	4.74	3.90	36000 s/93.8%	[9]
Co/N-C@CNFs	4.3, 3.2 $Co(NO_3)_2·6H_2O$ 2-methylimidazole	0.952	0.852	NR	4.20	70000s/92%	[16]
Co@N-C-1	NR, 12.12 $Co(OAc)_2$ urea	1.023	0.938	4.12	3.98	1000s/80%	[17]
Co-N-CNTs	0.59, 11.93 $Co(NO_3)_2·6H_2O$ 2-methylimidazole	0.974	0.853	NR	4.00	$\Delta E_{1/2}$=0 mV (10000 cycles)	[18]
Co@NC-ZM-900	0.61, 1.94 CoPc melamine	0.960	0.830	NR	4.18	20000 s/94.8%	[19]
Co-NOPC-600	8.74, 4.67 $Co(NO_3)_2·6H_2O$ 2-methylimidazole	0.950	0.860	5.20	3.93	86400s/85%	[23]
Co@NC/RGO-2.6	NR, NR $Co(NO_3)_2·6H_2O$ 2-methylimidazole	0.960	0.820	5.60	3.90	$\Delta E_{1/2}$= −2 mV (5000 cycles)	[24]
Co/N-C	0.68, 5.79 $Co(NO_3)_2·6H_2O$ 2-methylimidazole	0.877	0.817	5.11	3.65	36000s/87.1%	[25]

[1]NR=Not reported

Preprints (www.preprints.org) | NOT PEER-REVIEWED | Posted: 26 October 2021 doi:10.20944/preprints202110.0374.v1

[2]All catalysts measured in 0.1 M KOH solution.

[3]Co at.% and N at.% are tested by XPS.

[4] ppy-pani=polypyrrole-polyaniline

[5]EDTA-Co=ethylenediaminetetraacetic acid disodium cobalt salt hydrate

[6]DA=dopamine hydrochloride

4. Conclusion

In short, AC@CoPc series composite catalysts with nanoporous structure were prepared by through pre-activation treatment, high-temperature pyrolysis and precise control the composite proportion of AC and CoPc, in which the AC derived from biomass pine peel was served as carbon carrier compound with the nitrogen (N) source and inexpensive CoPc was served as the Co and N source. Compared with other AC@CoPc series composite catalysts and Pt/C (20%) catalyst, AC@CoPc-800-1-2 exhibits that the E_{onset} is 1.01 V and the stability is 87.8% in 0.1 M KOH. The high electrocatalytic activity of AC@PCo-800-1-2 composite catalyst can be attributed to the following three points. (i) AC derived from biomass pine peel is a kind of biomass carbon material with rich nanoporous structure and large SSA. When used as a carbon carrier, AC can not only provide more attachment sites for CoPc particles, but also can enhance the mechanical stability of the nanostructured composite material and prevent the agglomeration of composite catalyst particles. (ii) Heteroatom N-doped AC ameliorates the charge distribution of adjacent C atoms and optimizes the adsorption of key ORR intermediates, which greatly promotes O_2 adsorption and electron transfer. (iii) A reasonable composite proportion of AC and CoPc exposes more active sites, so that plentiful atomically dispersed Co nanoparticles encapsulated by graphitic carbon can be formed and synergistically with N promotes the exposure of CoN_x active sites. More importantly, taking the performance and price of the catalyst in practical application into account, this composite catalyst that directly obtains carbon materials from biomass and combines with phthalocyanine series compounds is likely to be widely used in nonprecious metal catalysts.

Author Contributions: Resources, data curation, investigation, writing-original draft, funding acquisition, writing-review & editing, Lei Zhao; data curation, investigation, writing-review & editing, Ziwei Lan; investigation, writing-review & editing, Junyu Su; writing-review & editing, Huazhu Liang; writing-review & editing,

Jiayu Yao; conceptualization, methodology, writing-review & editing, Wenhao Mo; conceptualization, methodology, supervision, writing-review & editing, Wenhu Yang; All authors have read and agreed to the published version of the manuscript.

Funding: This work was supported by the Zhanjiang Science and Technology Bureau (2019B01002) and Natural Science Foundation of Lingnan Normal University (ZL1004).

Data Availability Statement: Data is available on the request from the corresponding author.

Conflicts of Interest: The authors declare no conflicts of interest.

References

1. Venegas, R.; Muñoz-Becerra, K.; Candia-Onfray, C.; Marco, J.F.; Zagal, J.H.; Recio, F. Experimental reactivity descriptors of MNC catalysts for the oxygen reduction reaction. *Electrochim. Acta* **2020**, *332*, 135340.
2. Zhu, Y.; Lin, Q.; Hu, Z.; Chen, Y.; Yin, Y.; Tahini, H.A.; Lin, H.J.; Chen, C.T.; Zhang, X.; Shao, Z. Self‐Assembled Ruddlesden-Popper/Perovskite Hybrid with Lattice‐Oxygen Activation as a Superior Oxygen Evolution Electrocatalyst. *Small* **2020**, *16*, 2001204.
3. Tian, H.; Zhang, C.; Su, P.; Shen, Z.; Liu, H.; Wang, G.; Liu, S.; Liu, J. Metal-organic-framework-derived formation of Co–N–doped carbon materials for efficient oxygen reduction reaction. *Journal of Energy Chemistry* **2020**, *40*, 137-143.
4. Li, Y.-W.; Zhang, W.-J.; Li, C.-X.; Gu, L.; Du, H.-M.; Ma, H.-Y.; Wang, S.-N.; Zhao, J.-S. A dinuclear cobalt cluster as electrocatalyst for oxygen reduction reaction. *RSC Advances* **2019**, *9*, 42554-42560.
5. Liu, J.; Yu, H.-Y.; Zhang, T.-H.; Wang, W.-T.; Han, X.-F.; Yuan, Y.-X.; Yao, J.-L.; Yang, R.; Tian, J.-H. Honeycomb-like Self-Supported Co–N–C Catalysts with an Ultrastable Structure: Highly Efficient Electrocatalysts toward Oxygen Reduction Reaction in Alkaline and Acidic Solutions. *ACS Applied Energy Materials* **2021**,

4, 2522-2530.

6. Huang, Y.; Wang, Y.; Tang, C.; Wang, J.; Zhang, Q.; Wang, Y.; Zhang, J. Atomic Modulation and Structure Design of Carbons for Bifunctional Electrocatalysis in Metal-Air Batteries. *Adv. Mater.* **2019**, *31*, 1803800.
7. Tan, J.; He, X.; Yin, F.; Chen, B.; Liang, X.; Li, G.; Yin, H. Bimetallic ZnCo zeolitic imidazolate framework/polypyrrole-polyaniline derived Co/N-doped carbon for oxygen reduction reaction. *Int. J. Hydrogen Energy* **2020**, *45*, 15453-15464.
8. Li, Y.; Mo, C.; Li, J.; Yu, D. Pyrazine-nitrogen-rich exfoliated C_4N nanosheets as efficient metal-free polymeric catalysts for oxygen reduction reaction. *Journal of Energy Chemistry* **2020**, *49*, 243-247.
9. Zhang, B.; Le, M.; Chen, J.; Guo, H.; Wu, J.; Wang, L. Enhancing Defects of N-Doped Carbon Nanospheres Via Ultralow Co Atom Loading Engineering for a High-Efficiency Oxygen Reduction Reaction. *ACS Applied Energy Materials* **2021**, *4*, 3439-3447.
10. Wan, H.; Chen, F.; Ma, W.; Liu, X.; Ma, R. Advanced electrocatalysts based on two-dimensional transition metal hydroxides and their composites for alkaline oxygen reduction reaction. *Nanoscale* **2020**, *12*, 21479-21496.
11. Kuznetsov, D.A.; Han, B.; Yu, Y.; Rao, R.R.; Hwang, J.; Román-Leshkov, Y.; Shao-Horn, Y. Tuning Redox Transitions via Inductive Effect in Metal Oxides and Complexes, and Implications in Oxygen Electrocatalysis. *Joule* **2018**, *2*, 225-244.
12. Xu, Y.; Sumboja, A.; Zong, Y.; Darr, J.A. Bifunctionally active nanosized spinel cobalt nickel sulfides for sustainable secondary zinc-air batteries: examining the effects of compositional tuning on OER and ORR activity. *Catalysis Science & Technology* **2020**, *10*, 2173-2182.
13. Parra-Puerto, A.; Ng, K.L.; Fahy, K.; Goode, A.E.; Ryan, M.P.; Kucernak, A. Supported Transition Metal Phosphides: Activity Survey for HER, ORR, OER, and Corrosion Resistance in Acid and Alkaline Electrolytes. *ACS Catalysis* **2019**, *9*, 11515-11529.

14. Karuppasamy, K.; Prasanna, K.; Jothi, V.R.; Vikraman, D.; Hussain, S.; Hwang, J.-H.; Kim, H.-S. Recent Advances in Nanostructured Transition Metal Carbide- and Nitride-Based Cathode Electrocatalysts for Li-O_2 Batteries (LOBs): A Brief Review. *Nanomaterials* **2020**, *10*, 2106.
15. Prabhakaran, S.; Balamurugan, J.; Kim, N.H.; Lee, J.H. Hierarchical 3D Oxygenated Cobalt Molybdenum Selenide Nanosheets as Robust Trifunctional Catalyst for Water Splitting and Zinc-Air Batteries. *Small* **2020**, *16*, 2000797.
16. Meng, H.; Liu, Y.; Liu, H.; Pei, S.; Yuan, X.; Li, H.; Zhang, Y. ZIF67@MFC-Derived Co/N-C@CNFs Interconnected Frameworks with Graphitic Carbon-Encapsulated Co Nanoparticles as Highly Stable and Efficient Electrocatalysts for Oxygen Reduction Reactions. *ACS Applied Materials & Interfaces* **2020**, *12*, 41580-41589.
17. Wang, H.; Song, Y.; Cao, Y.; Yu, H.; Liang, H.; Peng, F. Facile Synthesis of Cobalt and Nitrogen Coordinated Carbon Nanotube as a High-Performance Electrocatalyst for Oxygen Reduction Reaction in Both Acidic and Alkaline Media. *ACS Sustainable Chemistry & Engineering* **2019**, *7*, 10951-10961.
18. Zhang, M.; Zhang, E.; Hu, C.; Zhao, Y.; Zhang, H.-m.; Zhang, Y.; Ji, M.; Yu, J.; Cong, G.; Liu, H.; et al. Controlled Synthesis of Co@N-Doped Carbon by Pyrolysis of ZIF with 2-Aminobenzimidazole Ligand for Enhancing Oxygen Reduction Reaction and the Application in Zn-Air Battery. *ACS Applied Materials & Interfaces* **2020**, *12*, 11693-11701.
19. Liu, H.; Wang, S.; Long, L.; Jia, J.; Liu, M. Carbon-nanotube-entangled Co,N-codoped carbon nanocomposite for oxygen reduction reaction. *Nanotechnology* **2021**, *32*, 205402.
20. Zhang, D.; Sun, P.; Zuo, Z.; Gong, T.; Huang, N.; Lv, X.; Sun, Y.; Sun, X. N, P-co doped carbon nanotubes coupled with Co_2P nanoparticles as bifunctional oxygen electrocatalyst. *J. Electroanal. Chem.* **2020**, *871*, 114327.
21. Wu, Z.-S.; Yang, S.; Sun, Y.; Parvez, K.; Feng, X.; Müllen, K. 3D Nitrogen-Doped Graphene Aerogel-Supported Fe_3O_4 Nanoparticles as Efficient Electrocatalysts for the Oxygen Reduction Reaction. *J. Am. Chem. Soc.* **2012**,

134, 9082-9085.

22. Gong, K.; Du, F.; Xia, Z.; Durstock, M.; Dai, L. Nitrogen-doped carbon nanotube arrays with high electrocatalytic activity for oxygen reduction. *science* **2009**, *323*, 760-764.
23. Qiao, M.; Wang, Y.; Mamat, X.; Chen, A.; Zou, G.; Li, L.; Hu, G.; Zhang, S.; Hu, X.; Voiry, D. Rational Design of Hierarchical, Porous, Co-Supported, N-Doped Carbon Architectures as Electrocatalyst for Oxygen Reduction. *ChemSusChem* **2020**, *13*, 741-748.
24. Gao, H.; Ma, Y.; Li, Y.; Cao, Y.; Yin, Z.; Luo, H.; Yan, J.; Zhang, Y. MOF-derived N-doped carbon coated Co/RGO composites with enhanced electrocatalytic activity for oxygen reduction reaction. *Inorg. Chem. Commun.* **2020**, *123*, 108330.
25. Liu, X.; Wang, L.; Zhang, G.; Sun, F.; Xing, G.; Tian, C.; Fu, H. Zinc Assisted Epitaxial Growth of N-Doped CNTs-Based Zeolitic Imidazole Frameworks Derivative for High Efficient Oxygen Reduction Reaction in Zn-Air Battery. *Chem. Eng. J.* **2020**, *414*, 127569.
26. Niu, H.-J.; Zhang, L.; Feng, J.-J.; Zhang, Q.-L.; Huang, H.; Wang, A.-J. Graphene-encapsulated cobalt nanoparticles embedded in porous nitrogen-doped graphitic carbon nanosheets as efficient electrocatalysts for oxygen reduction reaction. *J. Colloid Interface Sci.* **2019**, *552*, 744-751.
27. Praats, R.; Käärik, M.; Kikas, A.; Kisand, V.; Aruväli, J.; Paiste, P.; Merisalu, M.; Sarapuu, A.; Leis, J.; Sammelselg, V.; et al. Electroreduction of oxygen on cobalt phthalocyanine-modified carbide-derived carbon/carbon nanotube composite catalysts. *J. Solid State Electrochem.* **2021**, *25*, 57-71.
28. Kumar, A.; Gonçalves, J.M.; Lima, A.R.; Matias, T.A.; Nakamura, M.; Bernardes, J.S.; Araki, K.; Bertotti, M. Efficient and methanol resistant noble metal free electrocatalyst for tetraelectronic oxygen reduction reaction. *Electrochim. Acta* **2019**, *326*, 134984.
29. Debe, M.K. Electrocatalyst approaches and challenges for automotive fuel cells. *Nature* **2012**, *486*, 43-51.

30. Fan, L.; Su, X.; Cong, T.; Wang, Y.; Liu, C.; Xiong, Y. Co and N co-doped porous carbon derived from corn stalk core as electrocatalyst for oxygen reduction reaction in alkaline medium. *Int. J. Electrochem. Sci.* **2020**, 11723-11731.
31. Kim, S.; Park, H.; Li, O.L. Cobalt Nanoparticles on Plasma-Controlled Nitrogen-Doped Carbon as High-Performance ORR Electrocatalyst for Primary Zn-Air Battery. *Nanomaterials* **2020**, *10*, 223.
32. Xiao, C.; Luo, J.; Tan, M.; Xiao, Y.; Gao, B.; Zheng, Y.; Lin, B. Co/CoN_x decorated nitrogen-doped porous carbon derived from melamine sponge as highly active oxygen electrocatalysts for zinc-air batteries. *J. Power Sources* **2020**, *453*, 227900.
33. Chen, Y.; Wang, S.; Li, Z. A cobalt-pyrrole coordination compound as high performance cathode catalyst for direct borohydride fuel cells. *RSC Advances* **2020**, *10*, 29119-29127.
34. Huang, K.; Rong, C.; Zhang, W.; Yang, X.; Fan, Y.; Liu, L.; Yang, Z.; Chen, W.; Yang, J. MOF-assisted synthesis of Ni, Co, Zn, and N multidoped porous carbon as highly efficient oxygen reduction electrocatalysts in Zn-air batteries. *Materials Today Energy* **2021**, *19*, 100579.
35. Gong, X.; Peng, L.; Wang, X.; Wu, L.; Liu, Y. Duckweed derived nitrogen self-doped porous carbon materials as cost-effective electrocatalysts for oxygen reduction reaction in microbial fuel cells. *Int. J. Hydrogen Energy* **2020**, *45*, 15336-15345.
36. Hao, X.; Chen, W.; Jiang, Z.; Tian, X.; Hao, X.; Maiyalagan, T.; Jiang, Z.-J. Conversion of maize straw into nitrogen-doped porous graphitized carbon with ultra-high surface area as excellent oxygen reduction electrocatalyst for flexible zinc-air batteries. *Electrochim. Acta* **2020**, *362*, 137143.
37. Liu, X.; Yang, W.; Chen, L.; Liu, Z.; Long, L.; Wang, S.; Liu, C.; Dong, S.; Jia, J. Graphitic Carbon Nitride (g-C_3N_4)-Derived Bamboo-Like Carbon Nanotubes/Co Nanoparticles Hybrids for Highly Efficient Electrocatalytic Oxygen Reduction. *ACS Applied Materials & Interfaces* **2020**, *12*, 4463-4472.
38. Peng, J.-D.; Wu, Y.-T.; Yeh, M.-H.; Kuo, F.-Y.; Vittal, R.; Ho, K.-C. Transparent

Cobalt Selenide/Graphene Counter Electrode for Efficient Dye-Sensitized Solar Cells with $Co^{2+/3+}$-Based Redox Couple. *ACS Applied Materials & Interfaces* **2020**, *12*, 44597-44607.

39. Li, X.; Guan, B.Y.; Gao, S.; Lou, X.W. A general dual-templating approach to biomass-derived hierarchically porous heteroatom-doped carbon materials for enhanced electrocatalytic oxygen reduction. *Energy & Environmental Science* **2019**, *12*, 648-655.
40. Zhang, W.; Liu, X.; Gao, M.; Shang, H.; Liu, X. Co-Zn-MOFs Derived N-Doped Carbon Nanotubes with Crystalline Co Nanoparticles Embedded as Effective Oxygen Electrocatalysts. *Nanomaterials* **2021**, *11*, 261.
41. Chen, S.; Chen, S.; Zhang, B.; Zhang, J. Bifunctional Oxygen Electrocatalysis of N, S-Codoped Porous Carbon with Interspersed Hollow CoO Nanoparticles for Rechargeable Zn-Air Batteries. *ACS Applied Materials & Interfaces* **2019**, *11*, 16720-16728.
42. Zhang, W.; Xu, C.; Ma, C.; Li, G.; Wang, Y.; Zhang, K.; Li, F.; Liu, C.; Cheng, H.-M.; Du, Y.; et al. Nitrogen-Superdoped 3D Graphene Networks for High-Performance Supercapacitors. *Adv. Mater.* **2017**, *29*, 1701677.
43. Jaouen, F.; Herranz, J.; Lefèvre, M.; Dodelet, J.-P.; Kramm, U.I.; Herrmann, I.; Bogdanoff, P.; Maruyama, J.; Nagaoka, T.; Garsuch, A.; et al. Cross-Laboratory Experimental Study of Non-Noble-Metal Electrocatalysts for the Oxygen Reduction Reaction. *ACS Applied Materials & Interfaces* **2009**, *1*, 1623-1639.
44. Artyushkova, K.; Levendosky, S.; Atanassov, P.; Fulghum, J. XPS Structural Studies of Nano-composite Non-platinum Electrocatalysts for Polymer Electrolyte Fuel Cells. *Top. Catal.* **2007**, *46*, 263-275.
45. Arechederra, R.L.; Artyushkova, K.; Atanassov, P.; Minteer, S.D. Growth of Phthalocyanine Doped and Undoped Nanotubes Using Mild Synthesis Conditions for Development of Novel Oxygen Reduction Catalysts. *ACS Applied Materials & Interfaces* **2010**, *2*, 3295-3302.
46. Morozan, A.; Jégou, P.; Jousselme, B.; Palacin, S. Electrochemical performance of annealed cobalt-benzotriazole/CNTs catalysts towards the oxygen reduction

reaction. *PCCP* **2011**, *13*, 21600-21607.

47. Yan, J.; Meng, H.; Xie, F.; Yuan, X.; Yu, W.; Lin, W.; Ouyang, W.; Yuan, D. Metal free nitrogen doped hollow mesoporous graphene-analogous spheres as effective electrocatalyst for oxygen reduction reaction. *J. Power Sources* **2014**, *245*, 772-778.
48. Huang, H.; Lan, Z.; Li, W.; Mo, W.; Zhao, L.; Zhang, J. A novel and low-cost CuPc@C catalyst derived from the compounds of sunflower straw and copper phthalocyanine pigment for oxygen reduction reaction. *RSC Advances* **2021**, *11*, 15590-15597.